Structure and Ferromagnetism in Mn^{4+} Spinels: $AM_{0.5}Mn_{1.5}O_4$ (A = Li, Cu; M = Ni, Mg)

W. Branford[†] and M. A. Green*[,†,‡]

Davy Faraday Research Laboratory, Royal Institution of Great Britain, 21 Albemarle Street, London, W1X 4BS United Kingdom, and Department of Chemistry, University College London, 20 Gordon Street, London, WC1H 0AJ United Kingdom

D. A. Neumann

Center for Neutron Research, National Institute of Standards and Technology, Gaithersburg, Maryland 20899

Received September 21, 2001. Revised Manuscript Received December 4, 2001

The structure and electronic properties of a series of Mn^{IV} spinel oxides, with the general formula, $AM_{0.5}Mn_{1.5}O_4$ (A = Li, Cu; M = Ni, Mg), are investigated. These materials form an interesting analogy to pyrochlore structures that show colossal magnetoresistance properties. Studies of all the compounds show spontaneous magnetization at a well-defined transition temperature and their semiconducting nature.

Introduction

The transport properties of manganese oxides have proved to be a fruitful area of research in recent years. Of particular importance has been the observation of colossal magnetoresistance (CMR) in a number of perovskite and pyrochlore structures.[1−3] This phenomenon, whereby a large change in the electrical resistance is observed with the application of a magnetic field, is associated with a transition from the paramagnetic to ferromagnetic state.[4,5] It is extremely important in the development of new materials for the data storage industry. Most of the previous work was focused on mixed valence Mn^{III}/Mn^{IV} oxides with the perovskite structure, where the ferromagnetism is explained within the double-exchange mechanistic framework.[6] In this scheme, the ferromagnetic coupling between Mn^{III} and Mn^{IV} is mediated by electron hopping between the partially filled e_g orbitals of Mn^{III} and the empty e_g orbitals of Mn^{IV} with strong Hund's coupling. The parallel arrangement of the spins of the t_{2g} electrons reduces the energy barrier to transport in the ferromagnetic state, thus maximizing the electronic kinetic energy and lowering the overall energy of the system. Application of a magnetic field drives the system to order at higher temperature, shifting the temperature of the metal−insulator transition giving CMR around the Curie temperature.[2] Other mechanisms for CMR were shown to be possible with the observation of the effect in the pyrochlore, $Tl_2Mn_2O_7$.[7−12] In this material, the manganese is wholly in the integral oxidation state of 4+ and contains no e_g electrons and hence precludes double-exchange. In the pyrochlore system, the ferromagnetism is the result of a Mn−O−Mn superexchange interaction,[5] while the conduction band is primarily of thallium 6s character.[13] The CMR effect appears to be derived from an indirect scattering of the discrete ferromagnetic and conduction sublattices, resulting in hybridization of the Tl (6s), Mn (3d), and O (2p) orbitals.[14,13]

Transition metal oxides with the spinel structure, particularly ferrites, such as magnetite, have long been vital components for devices used in the magnetic storage of information.[15] The structure allows strong direct interactions between transition metal ions; thus, many, including $CoFe_2O_4$[16] and $BaFe_{12}O_{29}$,[17] are ferrimagnets with transition temperatures around room temperature. There are also examples of spinels exhibiting CMR, notably the chromium-based chalcogenides, $FeCr_2S_4$.[18] Magnetoresistance has also been reported in

* To whom correspondence should be addressed. E-mail: mark@ri.ac.uk.
† Royal Institution of Great Britain.
‡ University College London.

(1) Rao, C. N. R.; Mahesh, R. *Curr. Opin. Solid State Mater. Sci.* **1997**, *2*, 32.
(2) Rao, C. N. R.; Cheetham, A. K.; Mahesh, R. *Chem. Mater.* **1996**, *8*, 2421.
(3) Urushibara, A.; Moritomo, Y.; Arima, T.; Asamitsu, A.; Kido, G.; Tokura, Y. *Phys. Rev. B*: *Condens. Matter* **1995**, *51*, 14103.
(4) Wagner, P.; Gordon, I.; Das, A.; Vanacken, J.; Moshchalkov, V. V.; Bruynseraede, Y. *Int. J. Mod. Phys. B* **2000**, *14*, 3735.
(5) Majumdar, P.; Littlewood, P. B. *Nature* **1998**, *395*, 479.
(6) Zener, C. *Phys. Rev.* **1951**, *82*, 403.
(7) Mishra, S. K.; Satpathy, S. *Phys. Rev. B*: *Condens. Matter* **1998**, *58*, 7585.
(8) Majumdar, P.; Littlewood, P. *Phys. Rev. Lett.* **1998**, *81*, 1314.
(9) Hwang, H. Y.; Cheong, S. W. *Nature* **1997**, *389*, 942.
(10) Ramirez, A. P.; Subramanian, M. A. *Science* **1997**, *277*, 546.
(11) Shimakawa, Y.; Kubo, Y.; Manako, T. *Nature* **1996**, *379*, 53.
(12) Sushko, Y. V.; Kubo, Y.; Shimakawa, Y.; Manako, T. *Physica B* **1999**, *261*, 831.
(13) Shimakawa, Y.; Kubo, Y. *Mater. Sci. Eng., B* **1999**, *63*, 44.
(14) Imai, H.; Shimakawa, Y.; Sushko, Y. V.; Kubo, Y. *Phys. Rev. B* **2000**, *62*, 12190.
(15) Yu, Y.; Harrell, J. W. *IEEE Trans. Magn.* **1994**, *30*, 4083.
(16) Ding, J.; Chen, Y. J.; Shi, Y.; Wang, S. *Appl. Phys. Lett.* **2000**, *77*, 3621.
(17) Karim, R.; McKinstry, K. D.; Truedson, J. R.; Patton, C. E. *IEEE Trans. Magn.* **1992**, *28*, 3225.
(18) Ramirez, A. P.; Cava, R. J.; Krajewski, J. *Nature* **1997**, *386*, 156.

10.1021/cm010857a CCC: $22.00
Published on Web 03/12/2002

magnetite,[19,20] the inverse spinel $Fe^{3+}[Fe^{2+}Fe^{3+}]O_4$. In this structure, the ferromagnetic A and B sublattices, of d^5 ferric ion cores, are antiparallel, giving bulk ferrimagnetism. Above the Verwey transition, the minority spin B-site electron, derived from the Fe^{2+} ions, occupies a spin polarized t_{2g} band, giving poorly metallic conduction. The magnetoresistance is a result of different alignment of the ferrimagnetic moment in neighboring grains, causing extra scattering at the grain boundaries.[21]

The spinel structure, with general formula AB_2O_4, has many structural features common to the pyrochlore network;[22] the B cation sublattice is identical to that of the pyrochlore, though the difference in the oxygen positions results in a dissimilar B−O−B bond angle. Therefore, it may be possible to produce spinel-based materials with electronic features similar to $Tl_2Mn_2O_7$; that is, ferromagnetism caused by near 90° interactions and independent conduction from overlap between the metal ions on the tetrahedral site and the anions.

To pursue the analogy with the pyrochlore, it is necessary to have manganese(IV) ions on the B sublattice. If these octahedral sites were wholly occupied by Mn^{IV}, it can be seen clearly from charge neutrality principles that there can be no charge on the A site. This can be achieved by the delithiation of $LiMn_2O_4$ to form the metastable λ-MnO_2,[23] though it should be noted that delithiation is never complete, and a small amount of manganese(III) remains.[24] However, this material is insulating, as there is no A-site ion to form a conduction band. It is, however, possible to introduce a large amount of manganese(IV) to the B sites by balancing the charge with cations of low valency on the A site and a small proportion of the B sites. This is achieved in the series $AMn_{1.5}M_{0.5}O_4$ (A = Li or Cu and M = Ni or Mg) which is known to undergo a ferromagnetic transition at low temperatures,[25,26] but there has been little investigation into other physical property measurements. In this paper, we describe the structure and magnetic and transport properties of the spinel series $AMn_{1.5}M_{0.5}O_4$ (A = Li or Cu and M = Ni or Mg), which has a magnetic network similar to the pyrochlore $Tl_2Mn_2O_7$.

Experimental Section

Powder samples of composition $AB_{0.5}Mn_{1.5}O_4$ (A = Li, Cu; B = Mg, Ni) were produced by combining stoichiometric amounts of the relevant metal acetates, as in eq 1, with subsequent decomposition and firing. Reaction of the acetates was found to yield a more complete mixing and fewer impurities than the standard solid-state technique of grinding the appropriate oxides or carbonates together, at the relatively low reaction temperature. Specifically, in the reaction scheme given, when Li_2CO_3 and MnO_2 were used as starting materials, Bragg peaks assigned to the persistent impurity phase Li_2MnO_3 were identified in the product. The following reactions were carried out

$$A(CH_3CO_2)_2{\cdot}H_2O + 0.5B(CH_3CO_2)_2{\cdot}4H_2O + 1.5Mn(CH_3CO_2)_2{\cdot}4H_2O \rightarrow AB_{0.5}Mn_{1.5}O_4 + 12CO_2 + nH_2O \quad (A = Li, Cu; B = Mg, Ni, Co.) \quad (1)$$

The reaction mixture was ground thoroughly before decomposition, which was achieved by slowly heating the acetates from room temperature to 400 °C (ΔT = 0.7 °C/min). The product was then pelletized and fired at 750 °C for 4 days with intermittent regrinding. On completion of the synthesis, the reaction mixture was slow-cooled at 0.07 °C/min from 750 °C to room temperature to produce the final sample.[25] X-ray diffraction (XRD) data was collected on a Siemens D500 diffractometer fitted with a primary monochromator giving λ = 1.54056 Å. Magnetic susceptibility measurements were performed using a Quantum Design MPMS7 SQUID magnetometer. Magnetoresistance measurements were performed in an Oxford Instruments Maglab 2000 system. Neutron diffraction experiments were carried out on the BT1 constant wavelength diffractometer at the National Institute of Standards and Technology using a Cu(311) monochromator (λ = 1.5401 Å). Analysis of these data was performed by the Rietveld method[27] within the GSAS suite of software.[28]

Results

Structure. The XRD patterns confirmed the formation of monophasic, highly crystalline spinel phases for all compositions. There were, however, shoulders on the set of peaks {*hhl*} where $h + l = 2n$. This can be clearly seen in the XRD pattern of $LiMg_{0.5}Mn_{1.5}O_4$, shown in Figure 1. $LiMg_{0.5}Mn_{1.5}O_4$ and $CuMg_{0.5}Mn_{1.5}O_4$ exhibited cation ordering on the octahedral sites, resulting in a superstructure refined in the $P4_332$ space group. This ordering can be monitored by the emergence of low-angle peaks, indexed as (110), (210), and (211) in the XRD pattern. These reflections are forbidden in the more conventional spinel space group, $Fd\bar{3}m$, as face-centered symmetry results in the reflection condition (*hkl*): $h + k = 2n$, $h + l = 2n$, and $k + l = 2n$. This phenomenon was not apparent in the nickel-containing samples, whose XRD patterns could be satisfactorily fitted using the $Fd\bar{3}m$ space group. However, the absence of the low-angle reflections in the XRD patterns, as observed for $LiMg_{0.5}Mn_{1.5}O_4$ in Figure 1, is not conclusive evidence of cation disorder in the $ANi_{0.5}Mn_{1.5}O_4$ (A = Li or Cu) series of compounds, as nickel and manganese have similar numbers of electrons. Further information was obtained by neutron diffraction; the negative coherent scattering length of manganese (−3.73 fm) gives strong contrast with the other metals ions, particularly nickel (10.3 fm). The $CuNi_{0.5}Mn_{1.5}O_4$ powder neutron diffraction pattern was satisfactorily refined in the $Fd\bar{3}m$ space group, with manganese and nickel randomly distributed over the octahedral sites, giving an R_{wp} goodness-of-fit factor of 6.97%. However, it was found that a slight improvement in the fit was achieved by using a multiphase refinement using both the ordered ($P4_332$) and disordered ($Fd\bar{3}m$) structures. This resulted in reduction of the goodness-of-fit factor to 6.66%, where the second, or-

(19) Coey, J. M. D.; Berkowitz, A. E.; Balcells, L.; Putris, F. F.; Parker, F. T. *Appl. Phys. Lett.* **1998**, *72*, 734.
(20) Coey, J. M. D. *Philos. Trans. R. Soc. London, Ser. A* **1998**, *356*, 1519.
(21) Coey, J. M. D. *J. Appl. Phys.* **1999**, *85*, 5576.
(22) Wills, A. S.; Raju, N. P.; Greedan, J. E. *Chem. Mater.* **1999**, *11*, 1510.
(23) Greedan, J. E.; Liu, G.; Raju, N. P.; Reimers, J. N.; Tun, Z. *J. Appl. Phys.* **1996**, *79*, 6176.
(24) Greedan, J. E.; Raju, N. P.; Wills, A. S.; Morin, C.; Shaw, S. M.; Reimers, J. N. *Chem. Mater.* **1998**, *10*, 3058.
(25) Blasse, G. *J. Inorg. Nucl. Chem.* **1964**, *26*, 1473.
(26) Blasse, G. *Philips Res. Repts. Suppl.* **1964**, *20*, 1.
(27) Rietveld, H. M. *J. Appl. Crystallogr.* **1969**, *2*, 65.
(28) Larson, A. C.; von Dreele, R. B. *General Structure Analysis System*; Los Alamos National Laboratories: Los Alamos, NM, 1990.

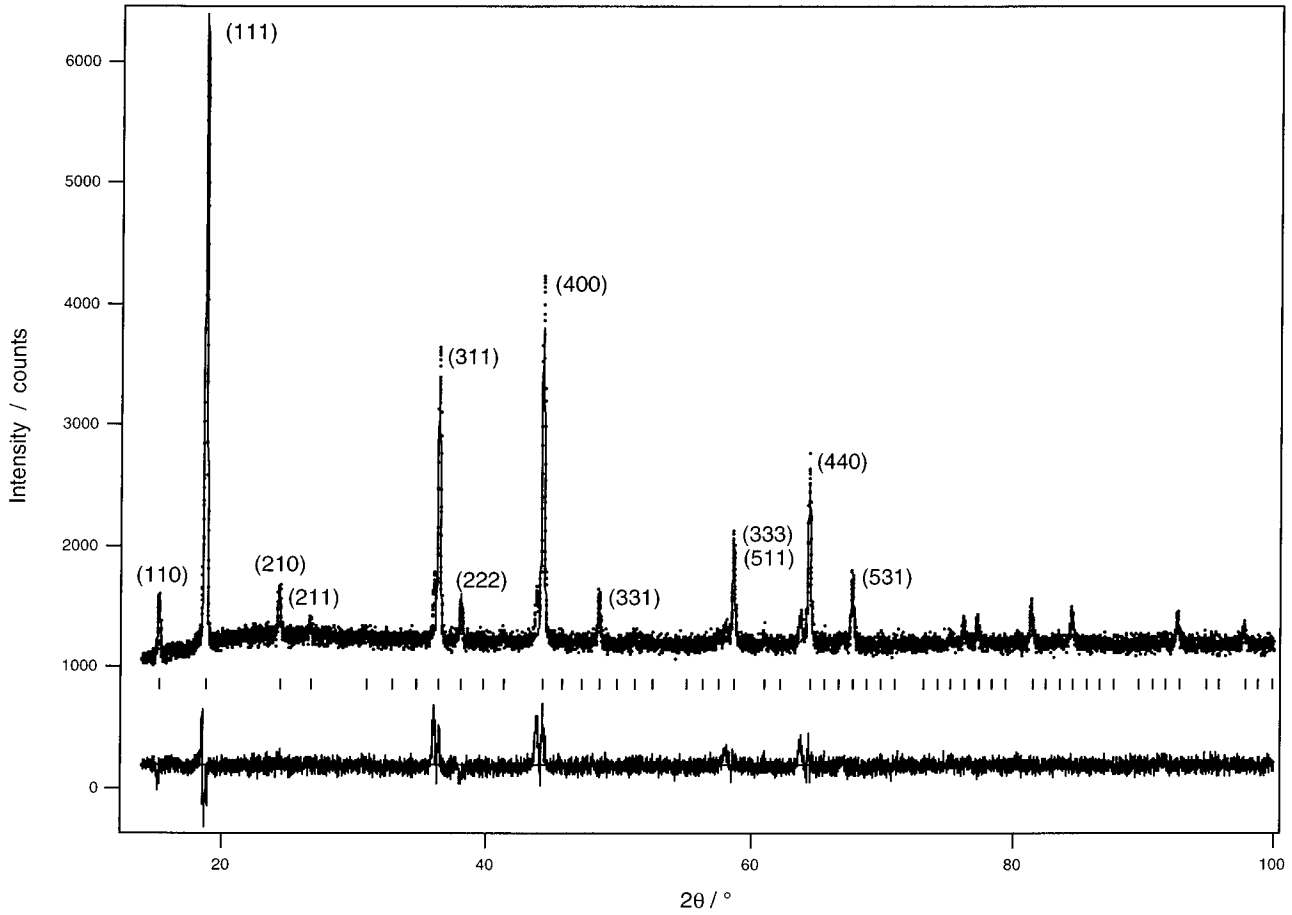

Figure 1. Rietveld refinement of the X-ray diffraction pattern of $LiMg_{0.5}Mn_{1.5}O_4$ using the $P4_332$ space group, where the Mg and Mn are ordering onto crystallographically distinct sites on the B sublattice.

dered phase was shown to be around 10% of the sample and had a marginally smaller lattice parameter. The resultant fit is shown in Figure 2. A summary of the structural parameters obtained in these measurements is given in Tables 1 and 2.

Magnetism. Figure 3 shows the magnetic susceptibility of the $A^{I}B^{II}_{0.5}Mn^{IV}_{1.5}O_4$ (A = Li, Cu; B = Mg, Ni) series. Each of the materials undergoes spontaneous magnetization from a paramagnetic state at a well-defined temperature. In the magnesium-containing compounds, the manganese ions are the only magnetic species and the behavior is ferromagnetic below the Curie temperature (T_c). The nickel-containing compounds constitute a more complicated set of interactions, as the Mn and Ni moments are expected to be antiferromagnetically coupled,[29,30] resulting in bulk ferrimagnetism. A consequence of this ferrimagnetic ordering can be seen in Figure 4; there is a reduction in the saturation magnetization in the nickel-containing compounds. The saturation moments of lithium and copper magnesium manganate are 2.263 and 2.387 μB/Mn, respectively; these are significantly greater than those of the nickel compounds, which are 1.958 and 1.964μB/Mn, respectively. These values are significantly below the theoretical spin-only values, which is typical of many spinel systems.[31]

The behavior of the ordering temperature is dependent on both the A- and B-site cations. The replacement of Li by Cu on the A site causes the T_C (or T_N) to increase by 15 K, whereas replacement of Mg with Ni causes it to increase by around 100 K. The variation in magnetic susceptibility above the ordering temperature provides another interesting comparison between the Mg and Ni analogues. All four compounds show close agreement with the Curie−Weiss law above their ordering temperatures, the results of which are shown in Table 3. For the Mg-containing samples, the Curie constants are close to the predicted spin-only value of 3.63 μ_B. However, for the Ni-containing samples, the Curie constants of only 1.445 for $CuNi_{0.5}Mn_{1.5}O_4$ and 1.620 for $LiNi_{0.5}Mn_{1.5}O_4$ are both far smaller than the predicted value of 5.15, assuming three unpaired electrons per manganese ion and two per nickel ion.

Low-temperature powder neutron diffraction was used to investigate the nature of the ferromagnetic ordering. The Rietveld refinement of $LiMg_{0.5}Mn_{1.5}O_4$ at 10 K, with and without a magnetic contribution, is presented in parts a and b of Figure 5. The magnetic model included is ferromagnetic with the moment aligned with one of the equivalent crystallographic axes, arbitrarily *z*. The refined moment on the 12d site was 2.167(50) μB, in good agreement with the saturation magnetic moment of 2.263 μB/Mn. The only significant magnetic contribution, to the 15 K powder neutron diffraction pattern of $CuNi_{0.5}Mn_{1.5}O_4$, is an increase in intensity in the (111) peak. This cannot be accounted

(29) Kanamori, J. *J. Phys. Chem. Solids* **1958**, *10*, 87.
(30) Blasse, G. *J. Phys. Chem. Solids* **1966**, *27*, 383.
(31) Valenzuela, R. *Magnetic Ceramics*; Cambridge: New York, 1994.

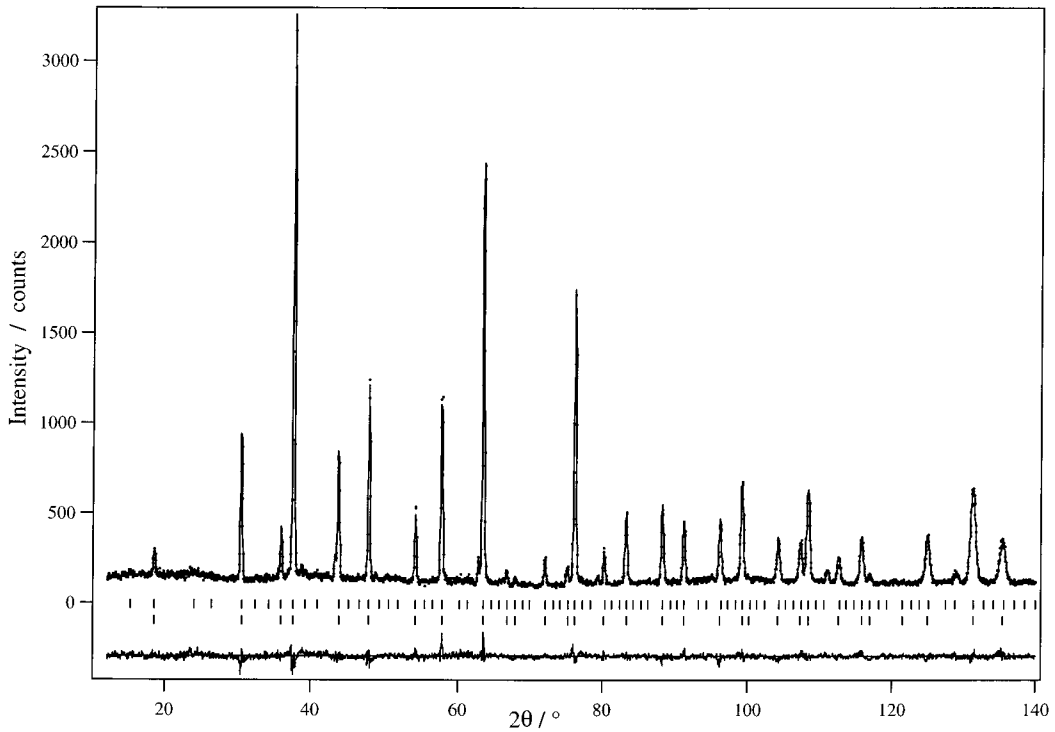

Figure 2. Rietveld refinement of the powder neutron diffraction pattern of $CuNi_{0.5}Mn_{1.5}O_4$, using a two-phase refinement, with the majority phase (~90%) in the $Fd\bar{3}m$ space group and an additional impurity phase in the ordered $P4_332$ space group.

Table 1. Structural Parameters Obtained from Rietveld Refinement of the Powder Neutron Diffraction Pattern of $LiMg_{0.5}Mn_{1.5}O_4$ at Room Temperature and 10 K and of $CuMg_{0.5}Mn_{1.5}O_4$ at Room Temperature; Space Group $P4_332$ Was Used with Positions A (*x*, *x*, *x*) (A = Li or Cu): Mg(1)/Mn(1) at (0.625, 0.625, 0.625), Mg(2)/Mn(2) at (0.125, *y*, *z*), and O(1) at (*x*, *x*, *x*) and O(2) at (*x*, *y*, *z*)

	site	Li (300 K)	Li (10 K)	Cu (300 K)
A	8c			
(*x*, *y*, *z*)		0.0028(11)	0.0048(8)	0.0057(2)
U/Å^2		0.0197(13)	0.0135(13)	0.0105(7)
Mg(1)	4b			
occupancy		0.959(10)	0.959(10)	0.953(9)
Mn(1)	4b			
occupancy		0.041(10)	0.041(10)	0.047(9)
Mn(1)/Mg(1) U/Å^2		0.0067(13)	0.0028(13)	0.0083(17)
Mg(2)/Mn(2)	12d			
y		0.3796(5)	0.3783(4)	0.3804(6)
z		0.8704(5)	0.8717	0.8696
Mg (2) occupancy		0.014(3)	0.014(3)	0.016(3)
Mn (2) occupancy		0.986(3)	0.986(3)	0.986(3)
Mn(2)/Mg(2) *U*/Å^2		0.0028(7)	0.0002(4)	0.0058(10)
O(1)	8c			
(*x*, *y*, *z*)		0.3833(2)	0.3837(2)	0.3850(3)
O(1) *U*/Å^2		0.0073(7)	0.0037(5)	0.0053(7)
O(2)	24e			
x		0.1512(2)	0.1505(2)	0.1493(3)
y		−0.1433(3)	−0.1434(3)	0.8585(2)
z		0.1235(3)	0.1233(3)	0.1271(3)
O(2) *U*/Å^2		0.0066(4)	0.0026(3)	0.0091(5)
a (= *b* = *c*)		8.18722(14)	8.18110(9)	8.28179(22)
R_{wp} (%)		10.41	7.56	8.19
χ^2		1.151	1.950	1.815

for with a purely structural model but was satisfactorily fitted with a magnetic model of collinear moments, along *z*, of 1.489(40) μB on each 16d site. This gave a goodness-of-fit factor of 6.09%. The saturation magnetization data discussed above clearly show that antiferromagnetic coupling between the Mn^{IV} and Ni^{II} ions results in bulk ferrimagnetism with a saturation moment of 1.964 μB/Mn, which is equivalent to 1.473 μB per B-site cation.

Table 2. Structural Parameters Obtained from Rietveld Refinement of the Powder Neutron Diffraction Pattern of $CuNi_{0.5}Mn_{1.5}O_4$ at Room Temperature and 10 K and from Powder X-ray Diffraction at Room Temperature for $LiNi_{0.5}Mn_{1.5}O_4$; Space Group $Fd\bar{3}m$ Was Used with Positions A at (0.125, 0.125, 0.125), B (Mn and Ni) at (0.5, 0.5, 0.5), and O at (*u*, *u*, *u*)

	site	Cu (300 K)	Cu (15 K)	Li (300 K)
A	8a			
U/Å^2		0.0117(5)	0.0074(3)	0.015(28)
Mn	16d			
occupancy		0.748(1)	0.748(1)	0.75[b]
Ni	16d			
occupancy		0.252(1)	0.252(1)	0.25[b]
Mn/Mg *U*/Å^2		0.0117(5)[a]	0.0074(3)[a]	0.070(10)
O	32e			
(*u*, *u*, *u*)		0.26314(6)	0.26323(5)	0.2632(7)
U/Å^2		0.01275(9)	0.0066(2)	0.088(29)
a (= *b* = *c*)		8.27858(11)	8.27127(8)	8.16594(3)
R_{wp} (%)		6.66	6.10	9.32
χ^2		1.232	1.741	1.028

[a] Constrained to A site value. [b] Not refined for X-ray data.

This collinear alignment in the best refinement is further indication that there is little or no ordering of the nickel and manganese ions on the length scale of neutron diffraction.

Conductivity. The plot of the natural logarithm of the resistance against 1/*T* for $LiNi_{0.5}Mn_{1.5}O_4$ is shown in Figure 6. The linear dependence of ln(ρ) with 1/*T* in the region of 270−350 K is consistent with a thermally activated semiconductor. The poor conductivity of this sample prevented the measurement of the resistance at low temperature due to a low carrier density, precluding measurement around the Curie temperature. Above the ordering temperatures, the resultant activation energies were determined to be 0.20(1) eV for $CuNi_{0.5}Mn_{1.5}O_4$, which is small compared to the 0.78(1) eV activation energy calculated for $LiNi_{0.5}Mn_{1.5}O_4$. Figure 7 shows the dependence of the resistivity of

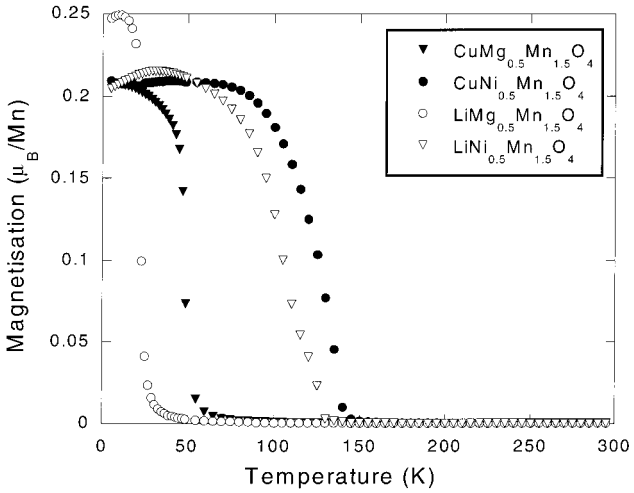

Figure 3. Molar magnetization of the $AB_{0.5}Mn_{1.5}O_4$ (A = Li, Cu; B = Mg, Ni) series as a function of temperature.

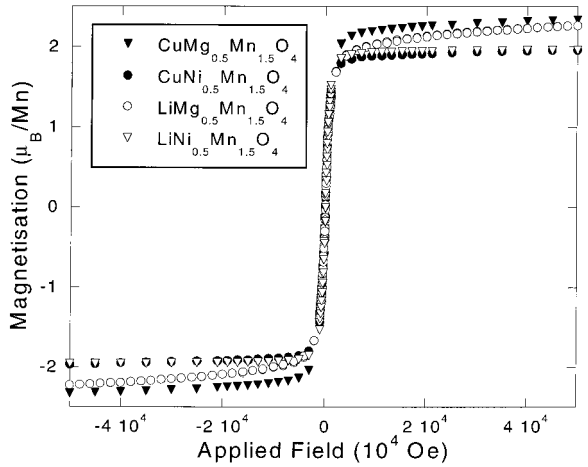

Figure 4. Molar magnetization of the $AB_{0.5}Mn_{1.5}O_4$ (A = Li, Cu; B = Mg, Ni) series as a function of applied field.

Table 3. Summary of the Result of Curie−Weiss Fits above the Ordering Temperature for the $AB_{0.5}Mn_{1.5}O_4$ (A = Li or Cu, B = Ni or Mg) Series of Compounds

compound	magnetic behavior	transition temp (K)	Curie constant	Weiss constant (K)
LiMg0.5Mn1.5O4	ferromagnetic	25	3.412(36)	37.6(1)
LiNi0.5Mn1.5O4	ferrimagnetic	110	1.620(10)	108.7(2)
CuMg0.5Mn1.5O4	ferromagnetic	50	3.207(11)	61.5(1)
CuNi0.5Mn1.5O4	ferrimagnetic	125	1.445(9)	141.48(13)

$CuNi_{0.5}Mn_{1.5}O_4$ on temperature in an applied magnetic field of 0, 10 000, and 25 000 Oe. The plots are almost overlapping with only small deviations at high temperature and a magnetoresistance effect, defined by $\rho(h) - \rho(0)/\rho(0)$, of around 2%. The temperature dependence of the resistivity changes dramatically at the Curie point of 150 K.

Discussion

The slow-cooling sample preparation was first reported by Blasse[25] and allows the formation of the cation-ordered form of $LiMg_{0.5}Mn_{1.5}O_4$, with crystallographically distinct manganese and magnesium sites. It also appears to favor the ordering of the stacking faults in the material, as the Warren peaks associated with the set of peaks $\{hhl\}$ where $h + l = 2n$ are much more pronounced than in the diffraction patterns of the quenched compounds. These systematic stacking faults in the cubic close-packed (ccp) oxide lattice are caused by the occurrence of a single layer of energetically similar hexagonal close-packed (hcp) oxide. The ABCABCA stacking of anion layers in the ccp system is perturbed to give an ABCABABCA defect. The slow-cooling has allowed these defects to order themselves over domains of the length scale of the diffraction experiments. This phenomenon has been previously reported in other $Fd\bar{3}m$ systems, such as diamond[32,33] and C_{70}.[34]

The Rietveld refinements of the neutron diffraction data show that, as expected from crystal field theory, the A sites are fully occupied by the monovalent ions, lithium or copper, and the cations with higher valency, magnesium, nickel, and manganese, occupy the octahedral B sites. It is worth noting here that electroneutrality could be satisfied with Cu^{2+} and an equal number of Mn^{3+} ions replacing Cu^+ and Mn^{4+}. These are both Jahn−Teller ions, and the lack of a distortion to tetragonal symmetry coupled with the similarity of the magnetization measurements (Figure 3) for copper and lithium analogues indicate that copper is present in the +1 oxidation state. This is also borne out by the Cu−O bond lengths: 1.9808(8) Å in $CuNi_{0.5}Mn_{1.5}O_4$ and a mean distance of 1.992(6) Å in $CuMg_{0.5}Mn_{1.5}O_4$. Taking a Shannon ionic radius of 1.24 Å for tetrahedral O^{2-}, the radii of the copper ions in the two samples are approximately 0.74 and 0.75 Å, respectively. The tetrahedral Shannon ionic radii for Cu^+ and Cu^{2+} are 0.74 and 0.71 Å, respectively.

It is somewhat surprising that the cation-ordered superstructure, observed for the Mg-containing compounds, is only observed as a minority phase in the neutron diffraction of $CuNi_{0.5}Mn_{1.5}O_4$. Gryffroy et al.[35] reported the presence of long-range order in $LiNi_{0.5}Mn_{1.5}O_4$ and only short-range cation ordering in $CuNi_{0.5}Mn_{1.5}O_4$, which was expressed as a modulation of the background in the powder neutron diffraction pattern. This therefore implies that presence of Li on the A site is more conducive to cation ordering than Cu. This might be due to the smaller lattice parameter in the lithium system. Though there is, clearly, some tendency to order in the Ni−Mn system, the ordering occurs far more readily in the Mg−Mn array, as is evidenced by the clear observation of superstructure in $CuMg_{0.5}Mn_{1.5}O_4$. For the ordered phase to be energetically favorable, the enthalpic gain must outweigh the entropic loss of the system. There are two potential driving forces for cation ordering on the B sublattice: size mismatch and charge difference. The disparity in charge is important, as an ordered scheme prevents the occurrence of regions with a non-zero net charge. This is probably the most important factor, but both the Ni and Mg ions have a +2 charge, so it does not explain the change in behavior. Thus, we must consider the relative sizes of the cations in question. Mn^{IV} is small, with an ionic radius of 67 pm. Both Ni^{II} and Mg^{II} are significantly larger than the Mn, at 83 and 86 pm, respectively, but

(32) Badzian, A.; Badzian, T. *Ceram. Int.* **1996**, *22*, 223.
(33) Takeuchi, S.; Suzuki, K. *Phys. Status Solidi A* **1999**, *171*, 99.
(34) Blanc, E.; Burgi, H. B.; Restori, R.; Schwarzenbach, D.; Ochsenbein, P. *Europhys. Lett.* **1996**, *33*, 205.
(35) Gryffroy, D.; Vandenberghe, R. E. *J. Phys. Chem. Solids* **1992**, *53*, 777.

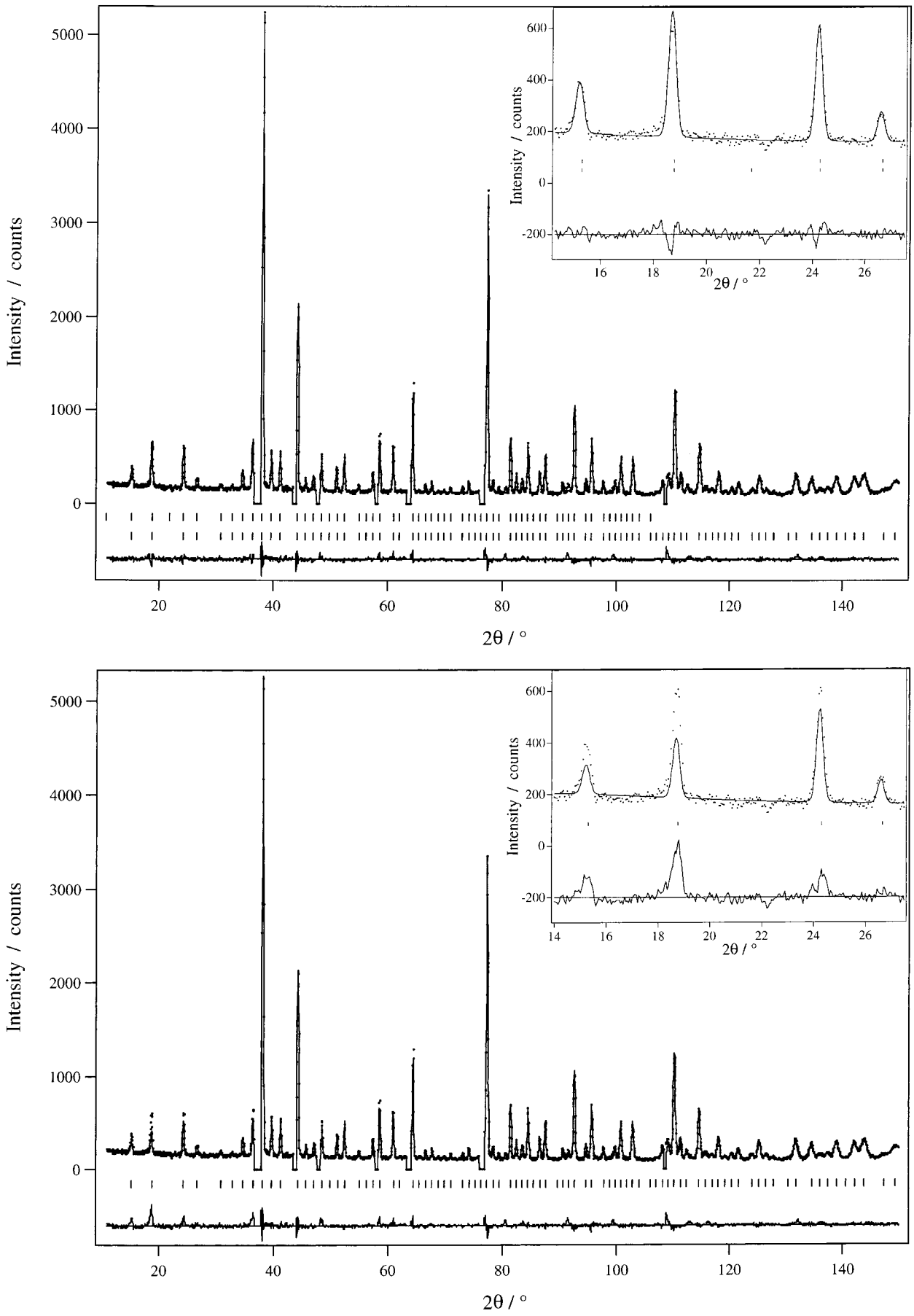

Figure 5. Rietveld refinement of the powder neutron diffraction pattern of $LiMg_{0.5}Mn_{1.5}O_4$ at 10 K with (a) a ferromagnetic phase included and (b) where no magnetic scattering is taken into account. The inset in both diagrams is an expanded region containing the low-angle data, showing significant improvement with the inclusion of the magnetic scattering.

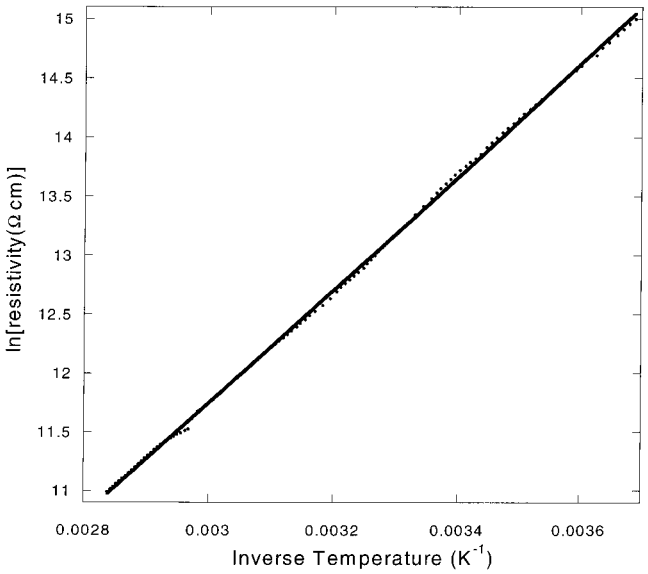

Figure 6. Natural logarithm of resistivity against inverse temperature for $LiNi_{0.5}Mn_{1.5}O_4$ in zero field; the straight lines show the fits to a semiconductive activation energy model of the resistance.

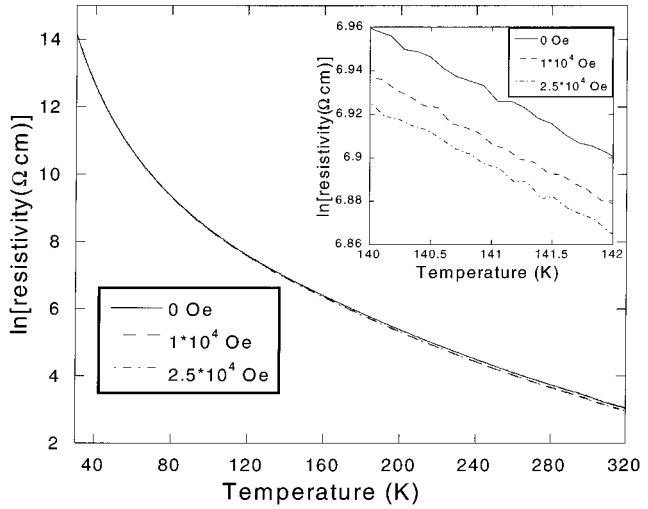

Figure 7. Natural logarithm of resistivity against temperature for $CuNi_{0.5}Mn_{1.5}O_4$ in three different applied magnetic fields of 0, 1×10^4, and 2.5×10^4 Oe.

are of similar magnitude; therefore, the difference in ordering behavior is not explained. However, the Ni^{II} is susceptible to oxidation to Ni(III), which is also stable in an octahedral environment. Therefore, the more likely cause of the reduced degree of cation ordering in the Ni-containing compound, in contrast to those containing Mg, is the occurrence of some degree of charge transfer. This reduces the difference in charge between ions on the same B site and therefore the susceptibility to cation order. The principal structural unit of the octahedral sublattice is the B_4O_4 cube, shown in Figure 8, which will be distorted from an ideal cube if the B cations are not all identical in size. These units are interlinked at the B-cation vertexes, and every unit will, if possible, have the same composition known as the Anderson condition.[36] These building blocks can pack together in the most efficient manner only if the large,

(36) Anderson, P. W. *Phys. Rev.* **1956**, *102*, 1008.

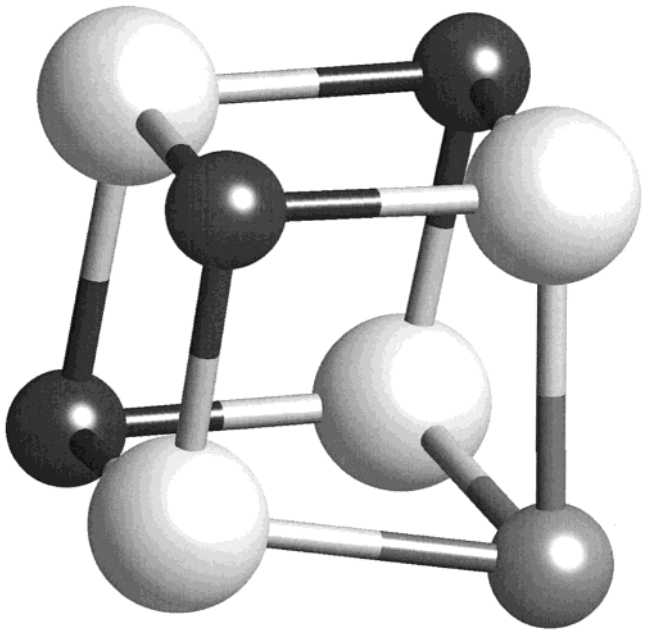

Figure 8. The main M_4O_4 structural unit of the AM_2O_4 spinel structure. These units are interlinked via the M atom vertexes. Mn_3MgO_4 from $LiMg_{0.5}Mn_{1.5}O_4$ at 10 K is shown. (Small black spheres are Mn; small gray spheres are Mg; large light spheres are O.)

low-valent, distortion-inducing cation is in the same position on each one. This is the origin of the cation ordering and the reason due to which the superstructures derived from ordering on the octahedral sites in the spinel structure are observed only when the stoichiometry can be represented with just four sites, that is, in 1:1 and 1:3 ratios only.

The magnetic behavior of both the spinel/pyrochlore system in general and these compounds in particular is complex. Goodenough[37] gave a qualitative interpretation of the various exchange interactions expected for a given exchange pathway and electronic configuration. However, there are often competing interactions of opposite sign, caused by the direct and superexchange pathways.[38] This makes it difficult to predict the overall sign of the exchange integral and causes superficially similar systems to exhibit markedly different magnetic properties. These compounds, $AB_{0.5}Mn_{1.5}O_4$, are considered with reference to the closely related compounds λ-MnO_2[24] and $Y_2Mn_2O_7$.[39,40] Both of these analogous compounds have a pyrochlorous magnetic lattice containing only manganese ions yet their bulk magnetic behavior is very different. At low temperatures, $LiMg_{0.5}Mn_{1.5}O_4$ is a ferromagnet, λ-MnO_2 is an antiferromagnet, and $Y_2Mn_2O_7$ is a spin glass with predominantly ferromagnetic interactions, as indicated by the positive Weiss constant ($\theta = +41$ K). It is appropriate to consider the magnetic trends within the series $AB_{0.5}Mn_{1.5}O_4$ before drawing conclusions about other structure types. The large variation in transition temperature within the series is indicative of a large change in superexchange

(37) Goodenough, J. B. *Magnetism and the Chemical Bond*; Interscience Publishers: New York-London, 1963.
(38) Motida, K.; Miyahara, S. *J. Phys. Soc. Jpn.* **1970**, *28*, 1188.
(39) Reimers, J. N.; Greedan, J. E.; Subramanian, M. A.; Kremer, R. K.; Gmelin, E. *J. Appl. Phys.* **1991**, *69*, 5255.
(40) Reimers, J. N.; Greedan, J. E.; Kremer, R. K.; Gmelin, E.; Subramanian, M. A. *Phys. Rev. B* **1991**, *43*, 3387.

energy between $LiMg_{0.5}Mn_{1.5}O_4$ ($T_C = 40$ K) and $CuNi_{0.5}Mn_{1.5}O_4$ ($T_N = 150$ K.) In all cases, the A cations are diamagnetic, so only B−B interactions need to be considered. The edge-sharing array of BO_6 octahedra results in a direct superexchange interaction of the d_{xy} (or d_{xz} or d_{yz}) orbitals of neighboring cations. In an ideal spinel, the nearest-neighbor B−O−B angle is 90°, but a distortion is often observed. For example, the B_4O_4 parallelepiped in $LiMg_{0.5}Mn_{1.5}O_4$ at 10 K has Mn−O−Mn angles of 94.91(15) and 99.25(22)° and an average Mn−O bond length of 1.907(4) Å. The magnesium(II) ion is also diamagnetic; therefore, in $LiMg_{0.5}Mn_{1.5}O_4$, the only exchange interaction is Mn(IV)−Mn(IV). The bulk magnetic properties make it clear that ferromagnetic oxygen-mediated superexchange overrides the antiferromagnetic direct exchange between t_{2g} orbitals. The most significant oxygen-mediated interaction is probably the nearest-neighbor $t_{2g}-p_x/p_y-t_{2g}$ superexchange,[41] though in $Y_2Mn_2O_7$, Reimers et al.[40] demonstrated that the coupling between nearest neighbors was negative (antiferromagnetic) but frustrated by ferromagnetic second and third neighbor interactions. It is immediately apparent from Figure 3 that substitution of magnesium with nickel has a large effect on the Curie temperature. This can be rationalized as there are now three superexchange interactions: the ferromagnetic Mn(IV)−Mn(IV) and Ni(II)−Ni(II) (not expected to be strong as the cation ordering results in all of the nickel ions with nearest neighbors being manganese ions) interactions and the antiferromagnetic Ni(II)−Mn(IV) interactions, giving ferrimagnetic order on the B sublattice. The strength of the superexchange interaction is dependent on the length of the B−O−B pathway; the B−O bond distance decreases with decreasing lattice parameter and increasing oxygen *u* parameter. It can be seen from the structural data in Tables 1 and 2 that in both the lithium and the copper analogues, the substitution of nickel for magnesium both decreases the lattice parameter and increases the *u* parameter. Thus, the great increase in T_C upon introduction of nickel can be wholly rationalized. A comparison of the copper and lithium compounds is less straightforward. Both are diamagnetic, so there are no new interactions, and a comparison of the structural parameters in Tables 1 and 2 shows that the substitution of lithium for copper has very little effect on the *u* parameter and expands the lattice parameter; thus, the B−O distance is increased. This decreases the B−O−B overlap and hence the strength of the ferromagnetic superexchange interaction, whereas the Curie temperature increases. It is now appropriate to consider the magnetic behavior of λ-MnO_2;[24] it was mentioned earlier that it possesses an identical B lattice, which is wholly occupied by manganese(IV) ions. Thus, it would be reasonable to expect similar behavior with a significantly higher transition temperature because there are no diamagnetic magnesium holes in the magnetic sublattice. It is, however, observed to be an antiferromagnet, the dominant interaction being the direct exchange between metal t_{2g} orbitals. Thus, in this system, the magnitude of the direct interaction is greater than that of the competing ferromagnetic exchange. If the effect of the magnesium "holes" is assumed to have a similar effect on both magnetic ordering schemes, then the key difference must be the Mn−Mn separation. The direct exchange interaction is extremely sensitive to this parameter, which determines the degree of t_{2g}:t_{2g} overlap, while the strength of the oxygen-mediated coupling is effective over larger distances. It should, however, be noted that the Mn−O−Mn bond angle is also highly significant. In $LiMg_{0.5}Mn_{1.5}O_4$, the Mn−Mn contact is between 2.867(4) and 2.923(4) Å and the Mn−O−Mn angle varies between 94.25(22) and 98.6(4)°. It has a slightly greater manganese separation than that quoted for λ-MnO_2 (2.84 Å) and a similar angle (96°). It is remarkable that a difference of only 1% in the Mn−Mn separation can result in such different magnetic behavior.

The conduction properties of these compounds are likely to be derived primarily from a Mn−O valence band and a Li/Cu−O conduction band. The high energy and small dispersion of this latter band result in no overlap with the Mn−O energy states, in contrast to the situation with the Tl−O and Mn−O bands of $Tl_2Mn_2O_7$, resulting in semiconducting properties. The Mn−O valence band also explains the different temperature variation of the resistance below T_c as long-range magnetic ordering would increase the localization and the energy barrier for the conduction process to take place.

Acknowledgment. This work was funded by the EPSRC (UK). Dr. C. Bellitto and Mr. F. Federici are thanked for help with the synthesis of $LiMg_{0.5}Mn_{1.5}O_4$. The National Institute of Standards and Technology (USA) is thanked for provision of neutron beam time. Certain commercial equipment, instruments, or materials are identified in this paper to adequately specify the experimental procedure. Such identification is not intended to imply recommendation or endorsement by the National Institute of Standards and Technology nor is it intended to imply that the materials or equipment identified are necessarily the best available for the purpose.

CM010857A

(41) Azzoni, C. B.; Mozzati, M. C.; Paleari, A.; Massarotti, V.; Capsoni, D.; Bini, M. *Z. Naturforsch., A: Phys. Sci.* **1998**, *53*, 693.